Journal of Chromatography A, 1231 (2012) 8–15

Contents lists available at SciVerse ScienceDirect

Journal of Chromatography A

journal homepage: www.elsevier.com/locate/chroma

Magnetic solid-phase extraction based on diphenyl functionalization of Fe_3O_4 magnetic nanoparticles for the determination of polycyclic aromatic hydrocarbons in urine samples

F. Bianchi [a,*], V. Chiesi [b], F. Casoli [b], P. Luches [c], L. Nasi [b], M. Careri [a], A. Mangia [a]

[a] Dipartimento di Chimica Generale ed Inorganica, Chimica Analitica, Chimica Fisica, Parco Area delle Scienze 17/A, 43124 Parma, Italy
[b] IMEM – CNR, Parco Area delle Scienze 37/A, 43124 Parma, Italy
[c] Centro S3 – Istituto Nanoscienze – CNR, via G. Campi 213/A, 41125 Modena, Italy

ARTICLE INFO

Article history:
Received 22 November 2011
Received in revised form 31 January 2012
Accepted 2 February 2012
Available online 13 February 2012

Keywords:
Magnetic nanoparticles
Solid-phase extraction
Polycyclic aromatic hydrocarbons
Gas chromatography–mass spectrometry

ABSTRACT

Superparamagnetic Fe_3O_4 diphenyl nanoparticles were prepared according to a solvothermal procedure and characterized by X-ray diffraction, infrared spectroscopy, surface area measurements, scanning electron microscopy, X-ray photoelectron spectroscopy and transmission electron microscopy. The magnetic phases present in the nanoparticle samples were analyzed by thermomagnetic analysis and the samples' magnetic properties were studied by vibrating sample magnetometry. The resulting nanoparticles having an average diameter of 200 nm were then used as solid-phase extraction sorbent for the determination of polycyclic aromatic hydrocarbons in urine samples. Method validation proved the feasibility of the developed beads for the quantitation of the investigated analytes at trace levels obtaining lower limit of quantitation values in the ng/l range. A good precision with coefficients of variations always lower than 15% was obtained. Finally, the superior extraction performance of the synthesized nanoparticles with respect to commercially available beads was proved.

1. Introduction

Recently, great attention has been paid to the synthesis of a variety of nanoparticles like spheres, nanotubes, nanocages and nanohorns using different materials, from silicon to iron oxide, from gold to carbon. Among them, magnetic nanoparticles have attracted broad attention due to their potential applications in magnetic resonance imaging [1], drug delivery [2] hyperthermia treatment [3] and analytical applications [4–6]. As for sample treatment procedures, superparamagnetic nanoparticles represent one of the most exciting prospects in analytical nanotechnology since they can be easily isolated from the matrix by using an external magnetic field without retaining residual magnetization after its removal. The main advantages over traditional solid-phase extraction sorbents rely on large surface areas, high extraction efficiencies, use of reduced amounts of sample and of toxic organic solvents. Different magnetic oxides have been synthesized using co-precipitation method [7], water-in-oil microemulsions [8], hydrothermal and solvothermal synthesis techniques [9–11]. Magnetite (Fe_3O_4) is the best-suited magnetic oxide for the above-cited applications, since it was widely characterized in the past and shows ferrimagnetic ordering at room temperature with a saturation magnetization of 92 emu/g [12]. Taking into account that electrical, optical and magnetic properties of nanoparticles strongly depend on their size, the synthesis of monodisperse nanoparticles with controlled particle sizes is of key importance [13–15]. In order to improve the selectivity of the extraction system, Fe_3O_4 nanoparticles can be also subjected to a proper surface functionalization. Magnetic nanoparticles characterized by a dual covalent immobilization of the matrix with probe proteins [16] and magnetic aptamer nanoparticles have been developed for the analysis of mannose in human plasma and peptides [4], respectively by using matrix-assisted laser desorption/ionization. Recently, silanes having different functional end-groups have been used in order both to increase their stability with respect to aggregation and to keep them well dispersed in aqueous media [17]. Octadecylsilane, n-octadecylphosphonic acid- and carbon-coated Fe_3O_4 nanoparticles have been proposed for the analysis of estrogens [18], polycyclic aromatic hydrocarbons (PAHs), phthalate esters [19–22] and ergosterol [23] in environmental samples and cigarettes, whereas cetyltrimethylammonium bromide-coated nanoparticles have been used for the pre-concentration of phenolic compounds [6].

In the field of human biomonitoring, the measurement of urinary metabolites represents a non-invasive approach to assess exposures resulting from different routes like inhalation, ingestion of contaminated food, dermal contact, etc. The exposure to PAHs

* Corresponding author. Tel.: +39 0521 905446; fax: +39 0521 905556.
E-mail address: federica.bianchi@unipr.it (F. Bianchi).

0021-9673/$ – see front matter © 2012 Elsevier B.V. All rights reserved.
doi:10.1016/j.chroma.2012.02.015

represents a matter of great importance in occupational health, since there is strong evidence that exposed people have increased risks of cancer [24]. PAHs have been frequently detected in urine as hydroxylated metabolites [25], being 1-hydroxypyrene commonly used to evaluate both the environmental and the occupational PAHs exposure. However, the determination of this metabolite can give only an indirect evaluation of the total exposure to PAHs mixture, thus requiring the monitoring of additional biomarkers. Taking into account that unmetabolized species are less susceptible to intra-individual variability and that their elimination is directly associated to previous exposure, a more useful approach for the biological monitoring of polycyclic aromatic hydrocarbons is represented by their determination as unmetabolized compounds. To our knowledge, only few studies dealing with the determination of unmetabolized PAHs in urine have been published [26–30]. More precisely, the developed methodologies were based on the use of solid-phase microextraction followed by GC–MS analysis and were applied to the determination of PAHs in the urine of coke-oven, asphalt roofing and road construction workers. However, taking into account that one of the major drawbacks related to the use of SPME is the possible degradation of the fiber when used for immersion analyses, all these studies except one were carried out using an headspace approach, not very suitable for the analysis of high-boiling PAHs. In this context, the development of alternative extraction/purification procedures as well as their miniaturization is of pivotal importance especially when low amounts of biological fluids like cerebrospinal fluid, infant plasma, serum, etc. need to be analyzed, thus proposing magnetic nanoparticles as one of the best choice to achieve in one step the extraction, purification and concentration of target analytes.

In this study we propose the preparation of diphenyl-functionalized magnetite nanoparticles and their potential application in the pre-concentration of unmetabolized urinary PAHs to evaluate the exposure of smoking people. To the best of our knowledge the use of magnetite nanoparticles for the extraction of PAHs from biological samples is proposed for the first time in this work.

2. Materials and methods

2.1. Reagents and materials

Iron(III)acetylacetonate ($Fe(acac)_3$, ≥99.9%, purity), tetraethoxysilane (TEOS, ≥99%, purity), benzyl alcohol (≥99%, purity), chlorodiphenylsilane (95%, purity), ethanol (≥99.5%, purity) dichloromethane (≥99.5%, purity) and triethylamine (≥99%, purity) were from Sigma–Aldrich (Milan, Italy). Toluene (99.7%, purity) was from Riedel-deHaën (Seelze, Germania). Hexane (97%, purity), ethanol (96%, purity) and ammonium hydroxide solution (28.0–30.0% NH_3 basis) were purchased from J.T. Baker (Deventer, The Netherlands).

PAHs [US Environmental Protection Agency (EPA) 525 PAH Mix B, 500 μg/ml each component in acetone] and [$^2H_{10}$]acenaphthene (acenaphthene-d_{10}), [$^2H_{10}$]phenanthrene (phenanthrene-d_{10}), [$^2H_{10}$]chrysene (chrysene-d_{10}) and [$^2H_{12}$]perylene (perylene-d_{12}), used as internal standards, were purchased from Supelco (Bellefonte, CA, USA). BcMag™ diphenyl magnetic beads were from Bioclone (San Diego, CA, USA).

PAH working solutions were prepared by proper dilution of the stock solution in blank urine.

2.2. Synthesis and functionalization of the magnetic nanoparticles

The synthesis of the magnetic nanoparticles was performed according to a previously developed procedure [31]. Briefly, 1 g of $Fe(acac)_3$ was added to 20 ml of benzyl alcohol and heated under nitrogen at 175 °C for two days. The resulting solution was centrifuged at 9000 rpm for 7 min and the precipitates washed several times with ethanol.

Subsequently, 30 mg of the obtained nanoparticles were dispersed in 80 ml of ethanol, followed by the addition of 5.3 ml of a 8 M ammonium hydroxide solution, 5 ml of bidistilled water and 100 μl of TEOS. The mixture was then stirred for 2 h at 50 °C and the particles dried under vacuum at 100 °C. Ninety ml of toluene were added to the obtained nanoparticles, followed by the addition of 10 ml of triethylamine and 1 ml of diphenychlorosilane. The mixture was refluxed for 2 days under stirring. Finally, the functionalized nanoparticles were centrifugated, collected by applying an external magnetic field and rinsed several times with hexane.

2.3. Characterization

X-ray powder diffraction (XRD) data were collected on a Thermo ARL X'TRA X-ray diffractometer CuKα X-radiation at a 40 kV and 30 mA.

Conventional and high-resolution transmission electron microscopy (TEM), as well as high angle annular dark field (HAADF) and energy dispersive X-ray spectroscopy (EDS) in scanning mode (STEM) were carried out on the solution of the nanoparticles using a JEOL2200FS microscope working at 200 keV. Samples were prepared by depositing a drop of a suspension of the particles in hexane on carbon-coated copper grids.

The magnetic critical temperatures were investigated by thermomagnetic analysis (TMA), which involves measuring the temperature dependence of the initial AC susceptibility of powder samples. The magnetic behavior of the nanoparticles was studied by vibrating sample magnetometry (VSM) on both powder samples and in solution in the temperature range 25 K to room temperature (RT).

Both magnetization curves and Zero Field Cooling (ZFC) and Field Cooling (FC) curves were measured. In a ZFC measurement, the sample is cooled in zero field and the magnetic moment at 100 Oe is then recorded as a function of increasing temperature. Afterwards, the sample is cooled to the minimum temperature in the presence of an applied field of 100 Oe and the moment is then recorded at the same field when heating the sample to RT (FC).

Infrared spectra were recorded using a FT-IR Nicolet Nexus spectrometer (Thermo Fisher Scientific, Waltham, MA, USA) between 4000 and 400 cm^{-1}.

Element analysis was performed on the CHNS-O Analyser FlashEA 1112 Series (CE Instruments, UK).

The XPS measurements were performed in a UHV system equipped with a conventional X-ray source (Al K_alpha photons) and a hemispherical analyzer, detecting the photelectrons at normal emission.

Surface area analysis was performed using a single point BET measurement on a Pulse Chemisorb 2705 unit (Micrometrics, Norcross, GA, USA). The total gas flow rate (30% N_2 in He) was maintained at 16 cm^3/min. Prior to surface area determination, the sample was pretreated in a flow of helium (30 cm^3/min) at 80 °C for 60 min.

2.4. GC–MS analysis

A HP 6890 Series Plus gas chromatograph (Agilent Technologies, Milan, Italy) equipped with a MSD 5973 mass spectrometer (Agilent Technologies) was used for GC–MS analysis. Helium was used as the carrier gas at a constant flow rate of 1 ml min^{-1}; the gas chromatograph was operated in splitless mode with the programmable temperature vaporization (PTV) injector (Agilent Technologies) maintained at the temperature of 310 °C and equipped with a

PTV multi-baffle liner (I.D. 1.5 mm, Agilent Technologies). The chromatographic separation of the PAHs was performed on a 30 m × 0.25 mm, d.f. 0.25 μm SLB-5MS capillary column (Supelco). The following GC oven temperature program was applied: 70 °C for 2 min, 15 °C min^{-1} to 190 °C, 10 °C min^{-1} to 290 °C, 290 °C for 5 min. Transfer line and source were maintained at the temperature of 280 and 250 °C, respectively. Preliminarily, full scan electron ionization (EI) data were acquired to determine appropriate masses under the following conditions: ionization energy: 70 eV, mass range: 35–350 amu, scan time: 3 scan/s. The mass spectrometer was finally operated in time-scheduled selected-ion monitoring (SIM) mode by applying a delay time of 4 min and by recording the current of the following ions: *m*/*z* 128, 127 and 102 for naphthalene from 4 to 7 min; *m*/*z* 152, 151 and 76 for acenaphthylene and *m*/*z* 154, 153 and 76 for acenaphthene and *m*/*z* 80, 162 and 164 for acenaphthene-d_{10} from 7 to 9.5 min; *m*/*z* 166, 165 and 139 for fluorene from 9.5 to 11 min; *m*/*z* 178, 176 and 152 for phenanthrene and anthracene and *m*/*z* 160, 184 and 188 for phenanthrene-d_{10} from 11 to 13 min; *m*/*z* 202, 200 and 101 for fluoranthene and pyrene from 13 to 16 min; *m*/*z* 228, 226 and 113 for benz[*a*]anthracene and chrysene and 120, 236 and 240 for chrysene-d_{12} from 16 to 18.5 min; *m*/*z* 252, 253 and 126 for benzo[*b*]fluoranthene, benzo[*k*]fluoranthene and benzo[*a*]pyrene and perylene-d_{12} from 18.5 to 21.5 min; *m*/*z* 279, 278, 276, 277, 139 and 138 for indeno[1,2,3-*cd*]pyrene, dibenzo[*a*,*h*]anthracene and benzo[*g*,*h*,*i*]perylene, from 21.5 to 25 min. For all the investigated analytes the corresponding ion ratios were used for confirmation purposes. A dwell time of 30 ms was used for all the ions. All the analyses were performed by setting the electron multiplier voltage at 2400 V.

Signal acquisition and data processing were performed using the HP Chemstation (Agilent Technologies).

2.5. Extraction

Twenty-five mg of nanoparticles were firstly activated with methanol and distilled water, then dispersed into 800 μl of blank urine spiked with the proper amounts of analytes. The mixture was then sonicated for 1 min: after 5 min of adsorption the nanoparticles were isolated by applying an external magnetic field and washed three times with 200 μl of toluene. One μl of this solution was then injected into the GC–MS system.

Finally, the developed procedure was applied to the analysis of five urinary samples of both smoking and no-smoking people and of no-smoking asphalt roofing workers. All the samples were stored at −18 °C until analysis.

2.6. Method validation

Method validation was carried out to meet the acceptance criteria for bioanalytical method validation [32]. Synthetic urine, obtained by dissolving proper amounts of salts and organic compounds in water was used as the matrix. The lower limits of quantification (LLOQs) were calculated as S/N = 5 using five independent samples and tested for accuracy and precision to meet the previously cited international criteria. The calibration curves were evaluated by analyzing synthetic urine spiked with the investigated analytes in the 0.3–30 ng/l range for naphthalene, acenaphthylene, acenaphthene, fluorene, phenanthrene, anthracene, pyrene, fluoranthene, benz[*a*]anthracene and chrysene and in the 0.5–30 ng/l range for benzo[*b*]fluoranthene, benzo[*k*]fluoranthene, benzo[*a*]pyrene, indeno[1,2,3-*cd*]pyrene, dibenzo[*a*,*h*]anthracene and benzo[*g*,*h*,*i*]perylene. Homoscedasticity was verified by applying the Bartlett test. Lack-of-fit and Mandel's fitting test were also performed to check the goodness of fit and linearity [33]. The significance of the intercept (significance level 5%) was established by running a Student's *t*-test. Intra-batch and inter-batch precision were calculated in terms of RSD% on three concentration levels (LLOQ, 5 and 30 ng/l) performing five replicates at each level. Accuracy was calculated in terms of recovery rate (RR%) on real urine samples as follows:

$$RR\% = \frac{c1}{c2} \times 100$$

where *c*1 is the measured concentration and *c*2 is the concentration calculated from the quantity spiked into the sample. Three different concentration levels (low, medium and high) with four replicated measurements were analyzed. The extraction yield in terms of percent recovery was calculated by comparing the results obtained from the magnetic extraction of standard solutions ($n = 3$) with those related to the analysis of urine samples containing the same amount of analytes ($n = 3$).

3. Results and discussion

3.1. Characterization of Fe_3O_4-diphenyl nanoparticles

TEM images of the obtained naked nanoparticles are shown in Fig. 1. These beads were characterized by an average diameter of 4 nm (Fig. 1A) and a spherical shape (Fig. 1B). In order to obtain

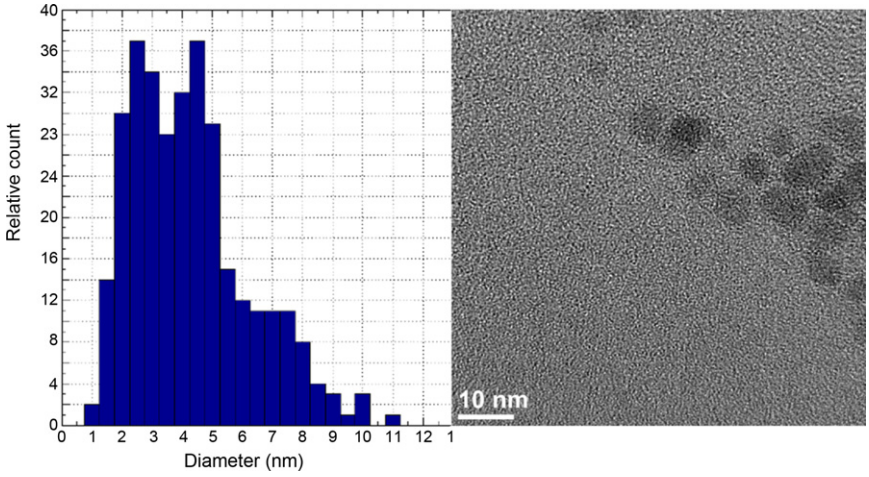

Fig. 1. (A) Particle size distribution histogram of magnetite nanocrystals based on the analysis of 324 nanoparticles. (B) TEM image of the nacked magnetic nanoparticles.

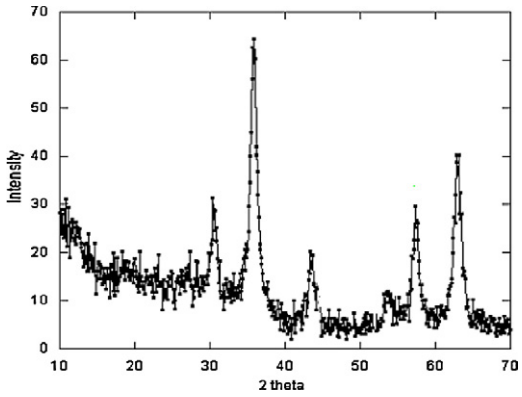

Fig. 2. XRD spectra of the naked Fe_3O_4 nanoparticles.

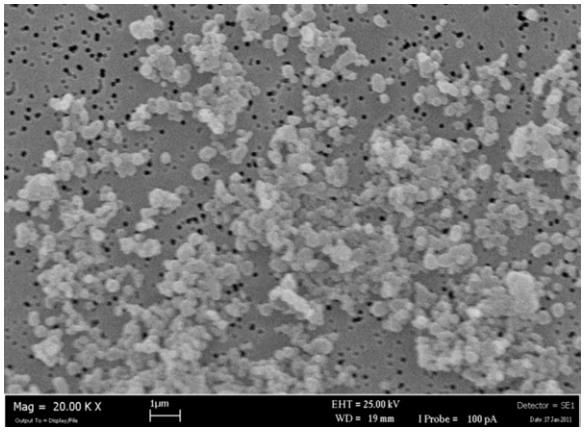

Fig. 5. SEM image of the functionalized nanoparticles.

reliable and statistically significant results hundreds of particles are counted and analyzed.

The synthesis of Fe_3O_4 was assessed both by means of XRD spectra and FTIR analysis. In the XRD spectra (Fig. 2) we observed the peaks corresponding to the (2 2 0), (3 1 1), (3 3 3), (4 0 0) and (4 4 0) reflections of Fe_3O_4 (JCPDS 82-1533).

The steps used for the subsequent functionalization of the nanoparticles using TEOS and chlorodiphenylsilane are reported in Fig. 3. As shown both in the STEM-HAADF image and in the corresponding EDX map (Fig. 4), the functionalization allowed to obtain spherical beads characterized by an average diameter of 200 nm constituted by an aggregation of synthesized nanoparticles surrounded by a diphenyl shell several tens of nm-thick. These results were also confirmed by SEM analysis (Figs. 4 and 5). The presence of a diphenyl coating was also proved by FTIR analysis. In fact, the FTIR spectra of naked Fe_3O_4 nanoparticles revealed the presence of absorption signals at 3400 cm^{-1} and 550 cm^{-1} corresponding to the O—H and Fe—O stretching vibrations, whereas signals at 1044 cm^{-1} corresponding to the Si—O stretching appeared after TEOS polymerization, thus indicating the successful silanization on the Fe_3O_4 surface. Finally, the disappearance of the stretching vibration of hydroxyl groups and signals at 3040 cm^{-1} and 1590 cm^{-1} corresponding to the aromatic C—H and C=C stretching vibrations, respectively were found in the case of diphenyl-based magnetic nanoparticles. To confirm the presence of magnetite, thermomagnetic analysis was also performed on Fe_3O_4-diphenyl nanoparticles. The TMA data (not shown here) evidence the Curie transition at 580 °C, typical of Fe_3O_4, and also a peak at 620 °C, corresponding to the Curie point of maghemite, i.e., γ-Fe_2O_3 [34]. Since a TMA measurement involves a thermal treatment up to 700 °C, it is impossible to establish if maghemite was present in the as-prepared samples or if it formed during the measurement. Therefore, even if the presence of a small fraction of maghemite in the sample cannot be excluded, TMA indicates that the magnetic oxides present in the sample are the best suited to the extraction procedure, being the saturation magnetization of both Fe_3O_4 and γ-Fe_2O_3 typically higher than 70 emu/g [35].

The magnetic properties of both the naked and diphenyl-coated nanoparticles were analyzed by measuring magnetization loops of

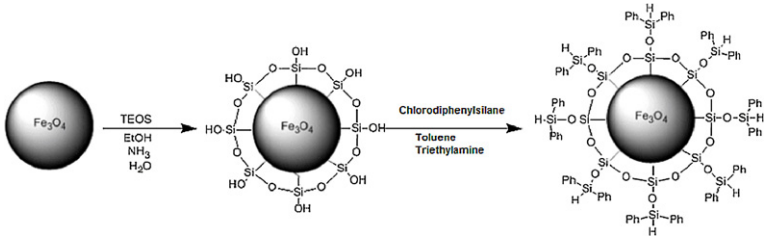

Fig. 3. Schematic representation of the functionalization process.

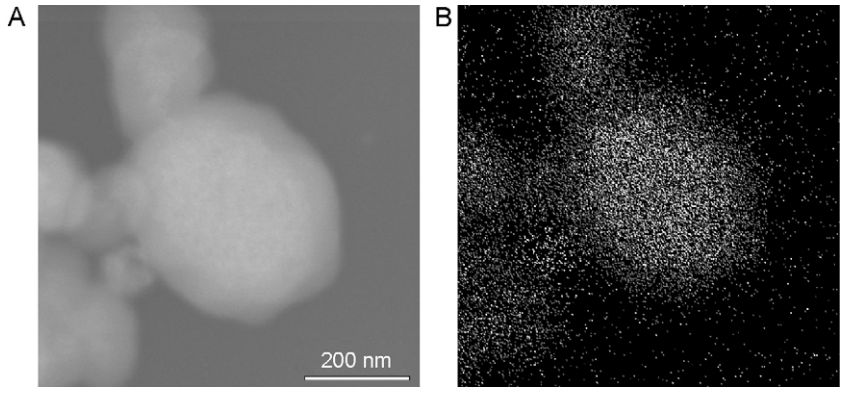

Fig. 4. (A) STEM-HAADF image and (B) the corresponding EDX map (Si: grey, Fe: white) of the functionalized nanoparticles.

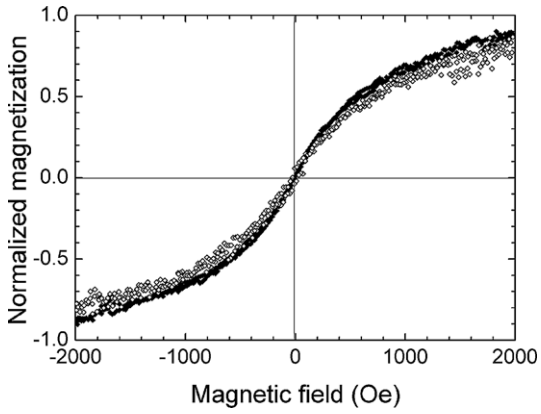

Fig. 6. Magnetization loops measured at 273 K on water colloidal suspensions of the naked (full symbols) and diphenyl-coated (open symbols) nanoparticles.

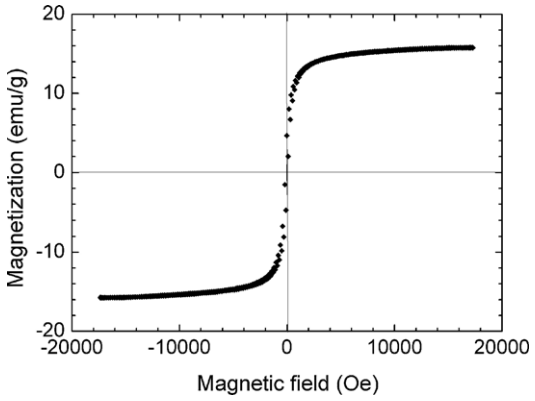

Fig. 8. Magnetization loop measured at room temperature on dried diphenyl-coated nanoparticles in a maximum applied field of 20 kOe.

colloidal suspensions. Both the samples show superparamagnetic behavior at 274 K, as evidenced by the absence of hysteresis in the loops reported in Fig. 6. This behavior guarantees the stability of the nanoparticles suspensions in ferrofluid state.

A more detailed investigation was performed on dried samples of the diphenyl-coated nanoparticles, which, due to the larger magnetic moment, allowed both the measurement of noiseless temperature-dependent properties at low applied field and an estimation of the magnetization value of the nanoparticles used for the extraction procedure. The Zero Field Cooling and Field Cooling curves, measured with a magnetic field of 100 Oe, are reported in Fig. 7. The ZFC curve shows a maximum around $T_B \cong 100$ K, corresponding to the average blocking temperature of the nanoparticles assembly. The ZFC and FC curves coincide above the irreversibility temperature T_{Irr} (≅140 K), thus for temperatures higher than T_{Irr} the magnetization process is perfectly reversible and the nanoparticles show a superparamagnetic behavior. T_{Irr} represents the maximum blocking temperature in the nanoparticles assembly.

The temperature dependence of relaxation time of magnetic moment is described by the Néel–Arrhenius law

$$\tau = \tau_0 \exp \frac{K_{eff} V}{K_B T} \quad (1)$$

where $K_{eff}V$ is the energy barrier proportional to the particle volume V and K_{eff}, which is the effective anisotropy constant. K_B is the Boltzmann constant.

Considering that the relaxation time of magnetic moments at the blocking temperature equals the time of the experiment, the average blocking temperature in a VSM measurement is related to the average volume through the equation [36]:

$$T_B = \frac{KV}{25K_B} \quad (2)$$

Using a K_{eff} value of 1.35×10^4 J/m^3 [37], an average radius of 8.5 nm can be estimated from equation (2). This result is in good agreement with TEM characterization, which shows naked nanoparticles with an average diameter of 4 nm. The estimated increase in nanoparticle size for the diphenyl-coated samples can be due to the formation of aggregates of more than one nanoparticle. Otherwise, the radius calculated from equation (2) for the coated-nanoparticles could be overestimated due to the hypothesis on K_{eff}, which could be enhanced due to the surface contribution.

The insets in Fig. 5 show the magnetization loops at RT and 28 K, typical of the superparamagnetic and ferromagnetic states, respectively. The coercive field evidenced at 28 K is 144 Oe, which is a typical value for magnetite/maghemite nanoparticles in the monodomain state [34].

The saturation magnetization (M_S) of diphenyl-coated nanoparticles was evaluated from the loop measured up to 18 kOe (Fig. 8). An M_S value of 16 emu/g at RT was obtained, by taking into account the Fe-oxide mass deduced from thermogravimetric analysis. The M_S value is much lower than the bulk value of magnetite, possibly due to an underestimation of the non-magnetic mass in the measured sample. Furthermore, the high surface-to-volume ratio of the nanoparticles can be partially responsible for the reduced magnetization. However the magnetization is sufficient to effectively isolate the nanoparticles from the matrix solution by means of an external magnetic field (Fig. 9).

The material was also characterized in terms of surface area, obtaining a value of 150 m^2/g.

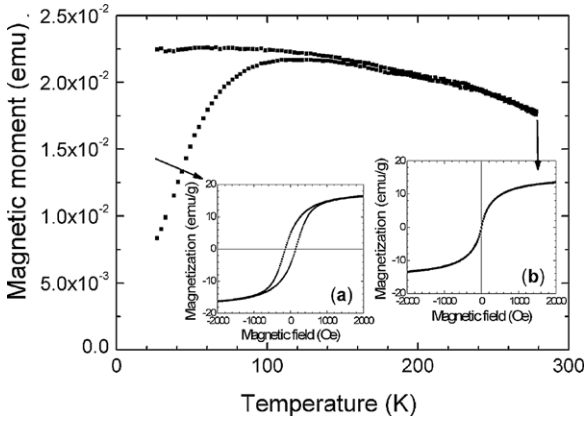

Fig. 7. ZFC and FC curves measured on dried diphenyl-coated nanoparticles under 100 Oe in the temperature range 28 K to RT. The insets represent the magnetization loops of the same sample at 28 K (a) and RT (b) in a maximum applied field of 2 kOe.

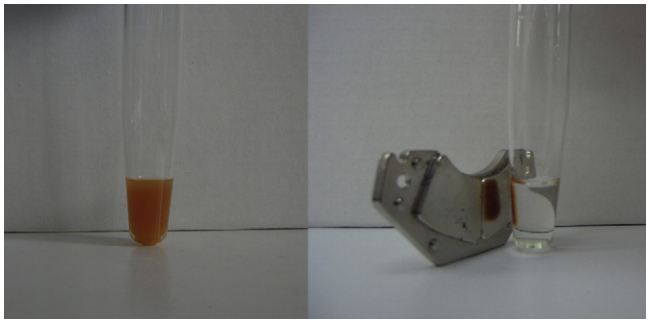

Fig. 9. Diphenyl Fe_3O_4 nanoparticles (left) dispersed in solution and (right) collected by a magnet.

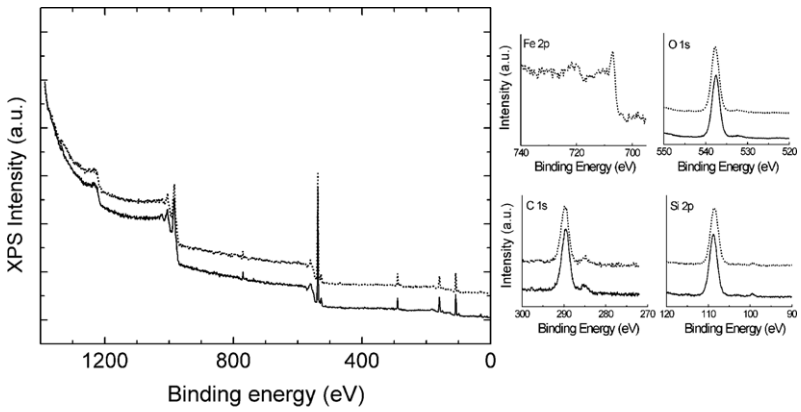

Fig. 10. XPS wide scans of diphenyl Fe_3O_4 nanoparticles in the as-prepared state (solid line) and after heating at 300 °C (dotted line). High resolution XPS spectra of Fe 2p, O 1s, C 1s and Si 2p are also reported.

Finally, the XPS characterization allowed to confirm the chemical structure of the nanoparticles. In Fig. 10 XPS spectra are reported, clearly showing Si 2p, C 1s and O 1s lines. Fe 2p line, detectable only after annealing the sample at 300 °C, is weaker compared to the other characteristic lines, since nanoparticles are buried under a diphenyl shell several tens of nm-thick. The shape of Fe 2p line and its satellites indicate that Fe oxide is present but do not allow to deconvolve magnetite and maghemite contributions.

3.2. Extraction of polycyclic aromatic compounds from urine

The capabilities of the magnetic nanoparticles were tested for the extraction of PAHs from urine. To our knowledge this is the first time that Fe_3O_4 nanoparticles are used for the extraction of these compounds from biological samples. Preliminary experiments were carried out in order to compare the results obtained from naked and diphenyl-based nanoparticles. The functionalization of the nanobeads allowed to perform a suitable extraction of the investigated compounds; by contrast, only unspecific adsorption of PAHs was observed when the naked Fe_3O_4 beads were used. Additional experiments were performed to improve the extraction efficiency of the analytes by evaluating the effect of some parameters able to influence the extraction yield like amount of sorbent, desorption solvent and extraction time. To evaluate the effect of the sorbent amount 5, 25 and 50 mg of diphenyl Fe_3O_4 nanoparticles were used. The presence of significant differences in the mean of the responses ($p < 0.05$) was observed by ANOVA: subsequently, multiple comparisons performed using the Bonferroni *t*-test revealed the absence of significant differences between the mean responses obtained using 25 and 50 mg of nanoparticles ($p > 0.05$), whereas significant differences were observed between the responses obtained using 5 vs 25 and 5 vs 50 mg of diphenyl Fe_3O_4 beads. On the basis of these findings, 25 mg were used for the study.

As for the extraction solvents, the extraction capabilities of toluene and hexane were investigated; as shown in Fig. 11A, toluene proved to be the best choice for the extraction of the 16 PAHs and this behavior can be explained on the basis of the presence of π–π interactions between the solvent and the aromatic rings of the analytes. The time of extraction was also evaluated in the 5–15 min range (Fig. 11B), showing that a time of 5 min was adequate to perform the extraction. These findings were very interesting especially if compared to those achieved in previous studies performed by means of SPME [26–30] and characterized by extraction times higher than 60 min. The rapid extraction time obtained in this study can be explained taking into account that the diphenyl beads, having an high surface area, were dispersed directly into the urine: by contrast, in the HS-SPME technique, the partition of PAHs into the gas phase requires longer extraction times. The extraction time was also more rapid than that used for direct immersion SPME as a consequence of the highest surface area of the diphenyl-nanobeads with respect to the SPME fiber. Finally, the performances of the synthesized nanobeads were compared with those of commercial devices (BcMag^{TM} diphenyl magnetic beads) evidencing the highest extraction capability of the developed nanoparticles with extraction yields ten times higher than those achieved using the commercially available beads. These findings can be explained taking into account the different size of the beads: in fact, the nanoparticles synthesized in laboratory were in the nanometer-scale range, whereas the commercial ones were in the micrometer-range, thus offering a reduced surface area for the interaction with the analytes.

3.3. Method validation and applications

The achieved results of the validation procedure are shown in Table 1. LLOQ values in the 0.04–0.39 ng/l range were obtained. These results are very satisfying being lower than those reported in previous studies for the analysis of unmetabolized PAHs in urine of exposed workers, obtained by using more conventional methods like SPME, both in the headspace and in immersion mode and showing LOQ values higher than 0.5 ng/l [26–30]. Again, the achievement of lower values in terms of limits of quantitation with respect to the HS-SPME procedure can be explained taking into account the highest extraction efficiency of the developed magnetic beads, thus confirming that the partitioning of the analytes into the headspace above the sample as the bottleneck of the technique. Again, the achieved results were also better than those obtained by means of SPME in the immersion mode as a consequence of the highest surface area of the diphenyl-nanobeads with respect to the SPME fiber.

Good linearity was observed for all the analytes in the 0.3–30 and 0.5–30 ng/l ranges by applying Mandel's fitting test. As for method precision, good results were achieved both in terms of intra-day and inter-day repeatability with RSD always lower than 15%. Extraction yields in the 56(±2)–112(±12)% and recoveries in the 88(±7)–97(±6)% ranges were obtained thus proving the accuracy of the developed method. In order to prove the reliability of the developed method the recoveries obtained using the magnetic extraction were compared with those achieved using SPME (immersion analyses) following the procedure described in a previous study [30]. As shown in Table 1 no significant differences were found between the recoveries of the utilized methods, thus proving the reliability of the developed nanoparticles for the extraction

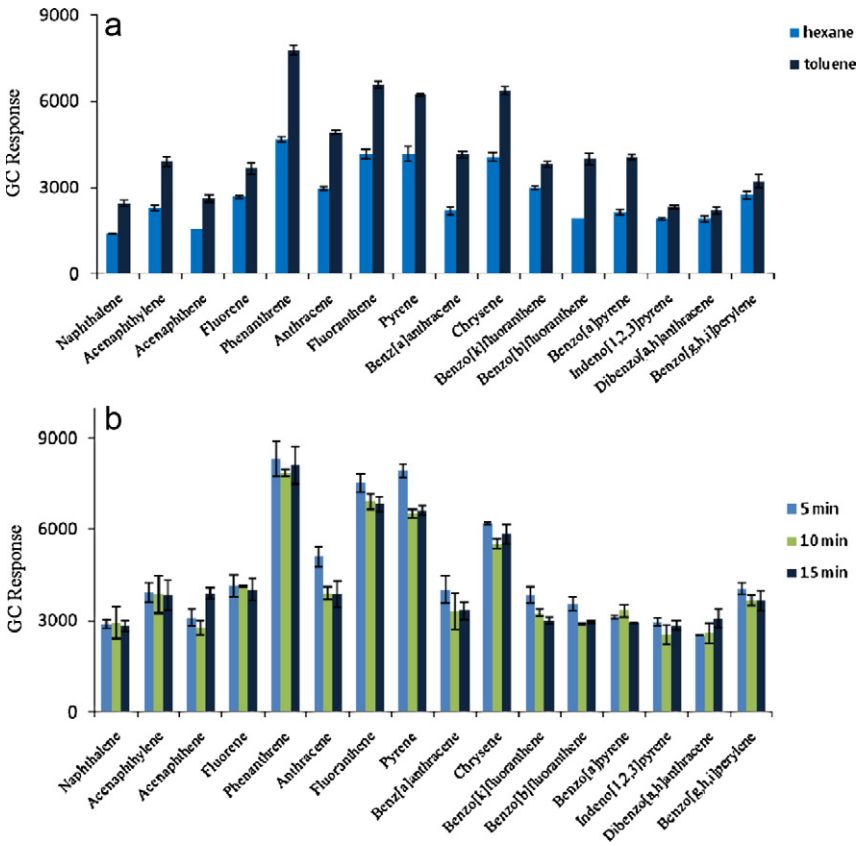

Fig. 11. Effect of: (A) extraction solvent and (B) extraction time. Sample: 800 μl of urine spiked with 1 μg/l of PAHs, 25 mg of diphenyl Fe_3O_4 nanoparticles, desorption solvent: 200 μl of hexane for three times.

of PAHs in biological samples. Finally, the method was applied for the analysis of urine samples of smoking and no-smoking people as well as of asphalt roofing workers (Table 2). As for the comparison between smoking and no-smoking people the obtained results showed that only naphthalene, acenaphthene, fluorene, phenanthrene and benz[*a*]anthracene could be detected at very low concentration levels in the urine samples of no-smoking people. By contrast, all the investigated compounds were found in the urine of smoking people with excretion values greater than those observed for no-smoking people.

However, the results obtained in the case of smoking people were significantly lower than those observed for occupationally exposed workers [26–30]. In fact, as shown in Table 2 all the 16 PAHs except for dibenzo[*a*,*h*]anthracene and benzo[*g*,*h*,*i*]perylene were detected in the urine of asphalt roofing workers at concentration levels at least two times higher than those observed in the case of smoking people. In addition the amount of sample required for the magnetic extraction is noticeably lower than that used when immersion SPME analyses were performed, thus suggesting that the developed diphenyl nanobeads can represent one of the most

Table 1
Validation parameters.

PAHs	LLOQ (ng/l)	Range (ng/l)	a ($\pm sd_a$)[a]	b ($\pm sd_b$)[b]	RR% nanobeads[c]	RR% SPME[c]
Naphthalene	0.04	0.3–30			88 ± 7	92 ± 5
Acenaphthylene	0.10	0.3–30	846 ± 23	–	92 ± 5	94 ± 4
Acenaphthene	0.14	0.3–30	669 ± 9	–	90 ± 3	87 ± 5
Fluorene	0.12	0.3–30	1079 ± 29	–	89 ± 6	90 ± 3
Phenanthrene	0.08	0.3–30	1609 ± 37	807 ± 119	94 ± 4	95 ± 4
Anthracene	0.11	0.3–30	1166 ± 14	–	89 ± 6	85 ± 5
Fluoranthene	0.06	0.3–30	1549 ± 39	–	97 ± 6	94 ± 4
Pyrene	0.04	0.3–30	1588 ± 43	–	95 ± 7	98 ± 4
Benz[*a*]anthracene	0.08	0.3–30	801 ± 28	–	93 ± 3	89 ± 5
Chrysene	0.09	0.3–30	1392 ± 56	–	89 ± 7	93 ± 3
Benzo[*b*]fluoranthene	0.33	0.5–30	847 ± 16	–	92 ± 6	88 ± 4
Benzo[*k*]fluoranthene	0.24	0.5–30	830 ± 51	912	91 ± 5	92 ± 5
Benzo[*a*]pyrene	0.38	0.5–30	753 ± 24	306 ± 79	95 ± 4	98 ± 5
Indeno[1,2,3-*cd*]pyrene	0.27	0.5–30	769 ± 13	–	90 ± 4	92 ± 5
Dibenzo[*a*,*h*]anthracene	0.39	0.5–30	726 ± 19	–	92 ± 3	94 ± 3
Benzo[*g*,*h*,*i*]perylene	0.24	0.5–30	1014 ± 27	–	91 ± 5	96 ± 5

[a] Regression: $y = ax + b$, confidence interval = 95%.
[b] Intercept not significant ($p > 0.05$).
[c] Urine samples spiked with 20 ng/l of PAHs.

Table 2
PAHs content in the urine of both smoking and no-smoking people and asphalt roofing workers.

PAHs	Smoking	No-smoking	Asphalt roofing workers
	Median (n = 5) ng/l		
Naphthalene	48.3	5	167
Acenaphthylene	1.5	n.d.	8.6
Acenaphthene	2.8	1.0	5.2
Fluorene	12.8	1.9	13.3
Phenanthrene	7	6.6	26.4
Anthracene	0.3	n.d.	7.1
Fluoranthene	5.3	n.d.	5.8
Pyrene	21.3	n.d.	32.8
Benz[*a*]anthracene	1.6	0.7	3.5
Chrysene	1.2	n.d.	3.8
Benzo[*b*]fluoranthene	0.6	n.d.	1.8
Benzo[*k*]fluoranthene	0.5	n.d.	1.6
Benzo[*a*]pyrene	<LLOQ	n.d.	0.8
Indeno[1,2,3-*cd*]pyrene	<LLOQ	n.d.	0.5
Dibenzo[*a*,*h*]anthracene	<LLOQ	n.d.	<LLOQ
Benzo[*g*,*h*,*i*]perylene	<LLOQ	n.d.	<LLOQ

n.d., not detected.

suitable extraction/pre-concentration technique for investigating the uptake of PAHs at very low concentration levels.

4. Conclusions

Magnetic nanoparticles were successfully synthesized and functionalized with diphenyl groups for the extraction of PAHs from urine of smoking and no-smoking people. Due to their Fe_3O_4 core, the nanoparticles could be easily isolated from the matrix by means of an external magnetic field. Compared with commercial devices, the nanometric size of the synthesized magnetic beads allowed to achieve superior extraction performances obtaining LLOQ values in the low ng/l range using a rapid and low-cost procedure.

References

[1] W.S. Seo, J.H. Lee, X.M. Sun, Y. Suzuki, D. Mann, Z. Liu, M. Terashima, P.C. Yang, M.V. Mcconnel, D.G.D.G. Niohimura, H.J. Dai, Nat. Mater. 5 (2006) 971.
[2] Y. Zhang, N. Kohler, M.Q. Zhang, Biomaterials 23 (2002) 1553.
[3] S. Morent, S. Vasseur, F. Grasset, E. Duguet, J. Mater. Chem. 14 (2004) 2161.
[4] K. Turney, T.J. Drake, J.E. Smith, W. Tan, W.W. Harrison, Rapid Commun. Mass Spectrom. 18 (2004) 2367.
[5] A.S. De Dios, M.E. Diaz-Garcia, Anal. Chim. Acta 666 (2010) 1.
[6] X. Zhao, Y. Shi, Y. Cai, S. Mou, Environ. Sci. Technol. 42 (2008) 1201.
[7] S. Qu, H. Yang, D. Ren, S. Kan, G. Zou, D. Li, M. Li, J. Colloid Interface Sci. 215 (1992) 190.
[8] N. Munshi, T.K. De, A. Maitra, J. Colloid Interface Sci. 190 (1997) 387.
[9] X. Wang, J. Zhuang, Q. Peng, Y.D. Li, Nature 437 (2005) 121.
[10] J. Park, K. An, Y. Hwang, J.G. Park, H.J. Noh, J.Y. Kim, J.H. Park, N.M. Hwang, T. Hyeo, Nat. Mater. 3 (2004) 891.
[11] G. Clavel, M.G. Willinger, D. Zitoun, N. Pinna, Adv. Funct. Mater. 17 (2007) 3159.
[12] J. Smit, H.P.J. Wijn, Ferrites, Philips Technical Library, Eindhoven, 1959.
[13] P. Guardia, N. Perez, A. Labarta, X. Batle, Langmuir 26 (2010) 5843.
[14] J. Park, E. Lee, N.M. Hwang, M. Kang, S.C. Kim, Y. Hwang, J.G. Park, H.J. Noh, J.Y. Kim, J.H. Park, T. Hyeon, Angew. Chem. Int. Ed. 44 (2005) 2872.
[15] M.V. Kovalenko, M.I. Bodnarchuk, R.T. Lechner, G. Hesser, F. Schaffler, W. Heiss, J. Am. Chem. Soc. 129 (2007) 6352.
[16] P.C. Lin, M.C. Tseng, A.K. Su, Y.L. Chen, C.C. Lin, Anal. Chem. 79 (2007) 3401.
[17] R. De Palma, S. Peeters, M.J. Van Bael, H. Van den Rul, K. Bonroy, W. Laureyn, J. Mullens, G. Borghs, G. Maes, Chem. Mater. 19 (2007) 1821.
[18] Y. Liu, L. Jia, Microchem. J. 89 (2008) 72.
[19] Y. Liu, H. Li, J.M. Lin, Talanta 77 (2009) 1037.
[20] L. Bai, B. Mei, Q.Z. Guo, Z.G. Shi, Y.Q. Feng, J. Chromatogr. A 1217 (2010) 7331.
[21] S. Zhang, H. Niu, Y. Cai, Y. Shi, J. Chromatogr. A 1217 (2010) 4757.
[22] S. Zhang, H. Niu, Y. Cai, Y. Shi, Anal. Chim. Acta 665 (2010) 167.
[23] Y. Sha, C. Deng, B. Liu, J. Chromatogr. A 1198–1199 (2008) 27.
[24] P. Boffetta, N. Jourenkova, P. Gustavsson, Cancer Causes Control 8 (1997) 444.
[25] M. Mattarozzi, M. Musci, M. Careri, A. Mangia, S. Fustinoni, L. Campo, F. Bianchi, J. Chromatogr. A 1216 (2009) 5634.
[26] L. Campo, R. Mercadante, F. Rossella, S. Fustinoni, Anal. Chim. Acta 631 (2009) 196.
[27] L. Campo, L. Addario, M. Buratti, L. Sciabetta, O. Longhi, C. Valla, P.E. Cirla, I. Martinotti, V. Foà, S. Fustinoni, Toxicol. Lett. 162 (2006) 132.
[28] S. Waidyanatha, Y. Zheng, S.M. Rappaport, Chem. Biol. Interact. 145 (2003) 165.
[29] L. Campo, F. Rossella, S. Pavanello, D. Mielzynska, E. Siwinska, L. Kapka, P.A. Bertazzi, S. Fustinoni, Toxicol. Lett. 192 (2010) 72.
[30] L. Campo, S. Fustinoni, P.A. Bertazzi, Anal. Chim. Acta 401 (2011) 625.
[31] N. Pinna, S. Grancharov, P. Beato, P. Bonville, M. Antonietti, M. Niederberger, Chem. Mater. 17 (2005) 3044.
[32] Guidance for Industry, Bioanalytical Method Validation, US Department of Health and Human Services, Food and Drug Administration, May, 2001.
[33] W. Funk, V. Dammann, G. Donnevert, Quality Assurance in Analytical Chemistry, VHC Publishers, New York, 1995.
[34] R.C. O'Handley, Modern Magnetic Materials. Principles and Applications, Wiley Interscience, New York, 2000.
[35] G. Bate, in: D.J. Craik (Ed.), Magnetic Oxides – Magnetic Properties, Wiley Interscience, London, 1975.
[36] B.D. Cullity, Introduction to Magnetic Materials, Addison-Wesley, Reading, MA, 1972.
[37] G.F. Goya, T.S. Berquò, F.C. Fonseca, J. Appl. Phys. 94 (2003) 3520.